



Coacervate or precipitate? Formation of non-equilibrium microstructures in coacervate emulsions

Journal:	<i>Soft Matter</i>
Manuscript ID	SM-ART-07-2023-000901.R1
Article Type:	Paper
Date Submitted by the Author:	08-Oct-2023
Complete List of Authors:	Edwards, Chelsea; UC Santa Barbara, Chemical Engineering Lakkis, Kareem; UC Santa Barbara, Chemical Engineering Luo, Yimin; University of California Santa Barbara, Mechanical Engineering and Materials Science Helgeson, Matthew; UC Santa Barbara, Chemical Engineering

Cite this: DOI: 00.0000/xxxxxxxxxx

Coacervate or precipitate? Formation of non-equilibrium microstructures in coacervate emulsions[†]

Chelsea E. R. Edwards^{ab}, Kareem L. Lakkis^a, Yimin Luo^{ab}, and Matthew E. Helgeson^{ab‡}

Received Date

Accepted Date

DOI: 00.0000/xxxxxxxxxx

Non-equilibrium processing of aqueous polyelectrolyte complex (PEC) coacervates is critical to many applications. In particular, many coacervate-forming systems are known to become trapped in out-of-equilibrium states (e.g., precipitation). The mechanism and conditions under which these states form, and whether they age, is not clearly understood. Here, we elucidate the influence of processing on the PEC coarsening mechanism as it varies with flow during mixing for a model system of poly(allylamine hydrochloride) and poly(acrylic acid sodium salt) in water. We demonstrate that flow conditions can be used to toggle the formation of rough, precipitate-like aggregates of micron-scale PEC structures. These structures form at compositions with viscous-dominant equilibrium rheology, and observations of their formation via optical microscopy suggest that they comprise colloidal aggregates of PEC coacervate droplets. We further show that these aggregates exhibit micron-scale coarsening, with a mixing time-dependent characteristic aging time scale. The results show that the formation of precipitate-like structures is not solely determined by composition, but is instead highly sensitive to mass transport and colloidal instability effects. Our observations suggest that the details of mixing flow can provide non-equilibrium structural control of a broad range of PEC coacervate materials orthogonally to structure-property inspired polymeric design. We anticipate that these findings will open the door for future studies on the control of non-equilibrium PEC formation and structure.

1 Introduction

Polyelectrolyte complexes (PECs) involve molecular association between charged macromolecules in solution due to opposite charge interactions. Coacervation occurs when these associations result in solution phase instability toward liquid-liquid phase separation (LLPS). Driven by counter-ion entropy and opposite-charge attraction of macro-ions, this LLPS results in the formation of PEC-rich condensates (usually as an emulsion-like suspension of coacervate droplets) in a PEC-poor dilute phase.

By contrast to the ordinary case of near-equilibrium coacervate emulsions in synthetic polyelectrolytes, cells and organisms in nature manipulate coacervation in time and space¹ to form a vast array of complex, out-of-equilibrium structures. These structures include dilute water-in-water emulsions of micron-scale droplets that buffer protein concentrations² or orchestrate biocatalysis,^{2–4} as well as PEC-rich droplets intended for processing or assembly into a high-performance soft material. Examples of the latter are ubiquitous, and include subcellular constructions^{1,2} such as

the mitotic spindle,⁵ to extracellular matrix,^{6,7} microtubules,⁸ byssal mussel plaque,⁹ polychaete jaw,¹⁰ snail mucus,¹¹ and spider silk.^{12,13} For this reason, PEC coacervate emulsion formation *via* LLPS has been identified as a facile and scalable route to assembling materials from both natural and synthetic polymers.

A critical step toward achieving synthetic replicates of these high-performance PEC materials is understanding and controlling coacervation behavior away from equilibrium, outside the cell. For example, they can adopt solid-like states whose formation conditions and mechanism remains unclear. Strategies to control non-equilibrium behavior of synthetic PEC coacervates remain primitive, with the exception of ATP-fuelled time control of LLPS in specific chemistries.¹⁴ In synthetic systems, the majority of coacervate research has aimed to characterize, model, and predict the complicated equilibrium phase behavior^{15–19} and equilibrium rheology^{20–27} of model coacervate-forming chemistries. Several pioneering studies established that titration order^{28–35} and mixing efficiency³⁶ of polyanion, polycation, and salt can affect molecular-level structure. However, the evolution from initial mixing to LLPS of PECs (i.e., emulsion formation)^{31,37–40} and their coarsening toward minimized surface energy (i.e., complete phase separation),^{35,41–43} and the structures that form *en route*^{26,34,42,44–46} still lack predictability beyond material-specific observations. Further, studies of coacervate formation in industry-relevant flow scenarios like shearing^{30,31}, spin coat-

^a Department of Chemical Engineering, University of California, Santa Barbara, CA 93106-5080 USA

^b Materials Research Laboratory, University of California, Santa Barbara, USA

[‡] E-mail: helgeson@ucsb.edu

[†] Electronic Supplementary Information (ESI) available: Table S1–S2; Figures S1–S8.

See DOI: 10.1039/cXsm00000x/

ing,⁶ and other physical mixing approaches^{34,35,38,45} do not consider that the properties of the flow encountered during mixing might affect the resulting PEC condensates' morphology and structure. An improved understanding of the effects of flow on the formation and aging of PEC materials could aid in their process design and scale-up, as well as in industrial processing of any polyelectrolyte-based formulation due to the prevalence of molecular polyelectrolyte complexation in such systems.^{47–50}

Recent studies on PEC formation often differentiate two subclasses of PEC condensates, coacervate and precipitate, based on their kinetic limitation: whereas "coacervate" is typically used to signify systems that achieve a viscoelastic liquid-like equilibrium state, "precipitate" is used to signify systems that appear to be trapped in a solid-like non-equilibrium state. In this work, we use the term "precipitate" to specifically distinguish PEC condensates with solid-like morphology or rheology.[†] Precipitates have macroscopic rheological signatures of either a glass^{51–55} or gel.^{20–22,56} Their microstructure forms an aggregated or "flaky" morphology at the microscale.^{57–63} By contrast, PECs classified as coacervates exhibit viscoelastic liquid-like rheology, which accompanies an aggregate-free droplet morphology. Current experimental literature distinguishes precipitate PECs from coacervate PECs using microscopy and rheological measurement as equally valid methods.^{60–63} The implicit assumption that enables this equivalence is that qualitatively distinct rheological behavior uniquely determines PEC morphology. This is an assumption we aim to test herein.

Additionally, the mechanisms of formation and coarsening of kinetically-trapped PEC condensates remains unclear. Existing experiments for PEC formation and growth only describe LLPS and classical liquid coarsening mechanisms such as coalescence. Current theories are unable to predict formation of kinetically-trapped states. Though precipitates and coacervates are thought to occupy mutually distinct regions of the salt-polymer-water phase diagram—with polymer chemistry determining the propensity to form precipitates at a certain composition^{20,52,57–59,62}—the connection between composition and the so-called "precipitation boundary" remains murky. A fundamental open question is how precipitate-like aggregates form and grow, and what determines their region of non-equilibrium formation within an equilibrium phase diagram.

In other colloidal systems, it is well-known that the presence of a flow field can induce aggregation in colloidal dispersions at high enough shear rates or concentrations.^{68,69} In this work, we specifically consider the possibility of whether precipitates in PEC coacervate suspensions can form in a similar way. If so, one could foreseeably identify processing guidelines to suppress or enhance kinetic trapping of PEC condensates in non-equilibrium states independently of their chemistry. Such guidelines would find applicability not only for lab-scale studies across chemistries, but also

for scalable engineering of PEC-based materials.

Finally, it remains unclear whether and how PEC precipitates age, and how exactly they are distinct from PEC coacervates. Pre-existing emulsions of protein condensates have been shown to eventually grow into solid amyloid fibrils at the proper compositions and chemistries.^{70–72} Conversely, some protein condensates have Maxwell fluid-like rheology that ages into a more solid-like one, as observed both *in vitro* and *in vivo* for a variety of evolutionarily distinct proteins.^{55,73,74} Whether pre-existing precipitates age has not been investigated to date. While none of the studied condensates are considered precipitates, nor do they form microscale aggregates, in our view these aging studies call into question the precise distinction between coacervate and precipitate, and at what length scale that distinction should be made.

Here, we explore the time-dependent formation and relaxation of PEC structure at the microscale. Using mixing flow-dependent studies on PEC coacervate formation, we develop an improved understanding of the PEC growth mechanism, and use this understanding to control it in a technologically-relevant flow scenario. In the process, we develop a nuanced view of the interplay between bulk rheology, mixing flow, and micron-scale aggregate formation in PEC condensates. Finally, by investigating how aggregated PEC microstructures age and coarsen after formation, we are able to develop a precise definition of a "precipitate" that accounts for flow effects and aging of the PEC properties.

2 Results

2.1 Flow induces aggregation in coacervate emulsions

As a model chemistry to investigate the effects of flow on PEC formation, we used mixed solutions of PAA and PAH (Figure 1A), at a 1:1 ratio of repeat units (r.u.) in Milli-Q water with added NaCl, with final pH 6.5.¹⁸ Following the pipette mixing protocol (see Section 5.3), mixing stock solutions to the desired total polyelectrolyte and salt concentration forms turbid mixtures indicative of PEC condensation. Observing these samples with optical microscopy confirms that microscale coacervate droplets, such as those shown in Figure 1B, generate turbidity at most state points. In salt-free samples, the turbidity is generated by a different microstructure identical to "precipitates" reported in the literature for the PAA-PAH system with the same chain lengths used herein.¹⁸ These precipitates have irregularly-shaped micron-scale structures⁶¹ that are visible to the naked eye when larger than 10s of microns⁷⁵ (~10s of individual droplets, see Section 2.2.1) as opaque, "flaky" flocculates.¹⁸

We discovered that flocs exhibiting the established morphological features of a precipitate can be generated by subjecting an existing coacervate emulsion to certain flow conditions (e.g. vortex mixing), without any change to the solution chemistry or composition (Figure 1C). Without sufficient flow conditions, coacervate emulsions did not otherwise form these structures. A typical micrograph of the floc structure is shown in Figure 1D. These flow-induced flocs can coexist with coacervate droplets. Based on the microstructural criterion for differentiating coacervate and precipitate morphologies,^{57–63} the flow-induced transition from droplets to amorphous aggregates indicates a transition from

[†] This definition is distinct from older literature, in which "precipitation" is used to signify molecular-level aggregation via polyelectrolyte complexation into amorphous aggregates of macro-ion pairs. This association of individual polyelectrolytes from a homogeneous solution is thought to occur prior to LLPS,^{28,64–66} as first proposed by Weiss and Aranyi.⁶⁷

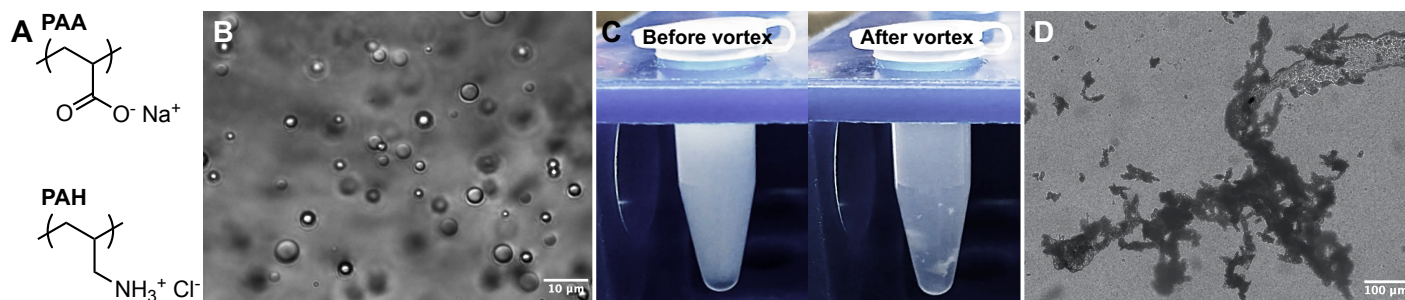


Fig. 1 Chemistry, microstructures, and flow-sensitivity of PAA-PAH PECs. (a) Chemical structure of the polyelectrolytes used herein. (b) Droplet microstructure of a PAA-PAH coacervate emulsion. (c) Vortex mixing the emulsion results in floc formation and a decrease in background turbidity at certain compositions (see Figure 2). (d) Aggregated microstructural morphology is indicative of a precipitate, and typical for vortex-induced PEC flocs.

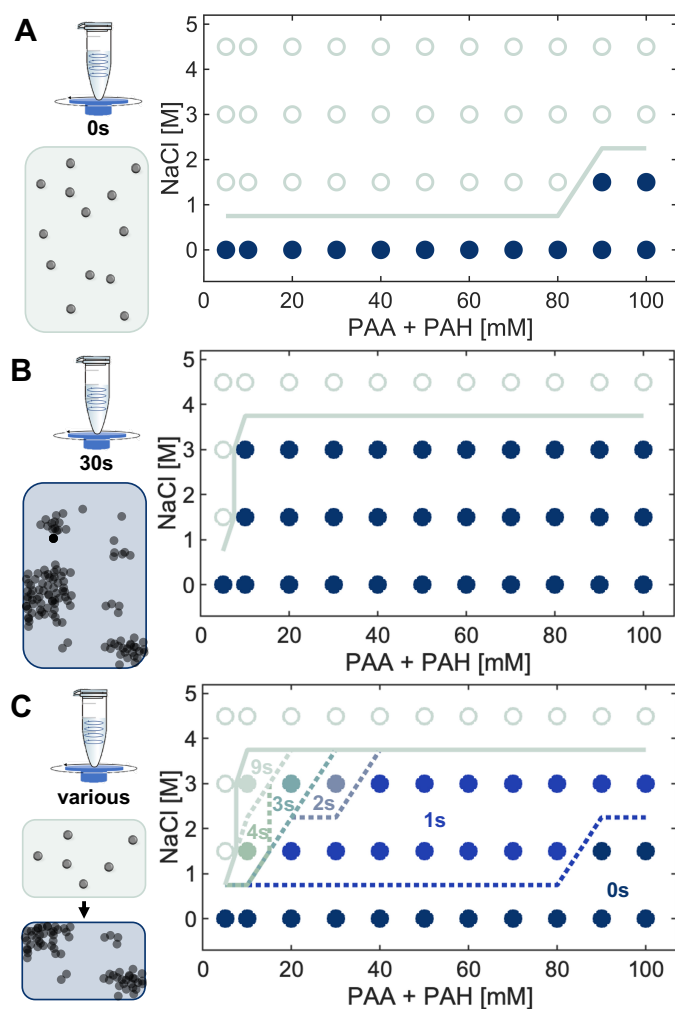


Fig. 2 Precipitation boundary for PAA-PAH is strongly sensitive to mixing flow. Filled symbols indicate the presence of visible flocs, consistent with Figure 1C. Open circles represent compositions without visible aggregates (no flocs); all compositions are within the two-phase region (see Figure S1 for phase diagram). (a) State diagram for PAA-PAH PEC morphology after pipette mixing (0 s vortex), with schematic of the dominant microstructural morphology (droplets) at left. (b) State diagram after an additional 30 s vortex, with schematic of the dominant microstructural morphology (flocs). (c) Compilation of state diagrams after vortex mixing for various durations reveals a transition from droplet-only systems to floc formation with increasing vortex time, as indicated (navy - no vortex mixing; blue - 1 s vortex mixing; etc.).

coacervate to precipitate initiated entirely by flow. This result constitutes the first demonstration of modulating the PEC condensate morphology using a non-chemical handle: prior works assume chemistry or component composition are the primary driver for initiating the coacervate-precipitate transition.^{18,20,57–59,61}

Coexistence of coacervate and precipitate microstructures herein suggests that the PAA-PAH precipitate boundary is actually a transition region, in contrast to rheologically-determined coacervate-precipitate boundaries that categorically delineate liquid and solid PEC properties. Further, flow-induced floc formation suggests the boundary for PAA-PAH precipitate formation is sensitive to sample preparation protocols. For example, we find that—for most compositions—the amount of time that an existing PEC emulsion is subjected to vortex mixing determines whether or not mixing-induced flocs form at that particular composition (Figure 2). The range of preparation compositions shown in Figure 2 relative to the experimentally-determined PAA-PAH equilibrium phase boundary is shown in Figure S1.

The flocculation boundary is detected by visual observation immediately after mixing, since turbidimetry cannot differentiate samples containing coexistent precipitate with reasonable statistics due to its convoluted dependence on the size, concentration, and internal composition/index contrast of PECs. Additionally, as compared to optical microscopy, visual inspection is a viable alternative for detecting finely-tuned differences in aggregation behavior between seconds of vortex time at higher salt concentrations, due to the time lag and sample manipulation required to transfer samples from microcentrifuge tubes to the optical microscope (see Section 5.4). Shifts in the aggregate-coacervate boundary are repeatable ($n = 4$) for a given mixing duration by multiple experimentalists.

As vortex duration is increased, flocs form at a wider range of compositions, and the location of the precipitate-coacervate boundary expands toward lower repeat unit (r.u.) polymer concentration and higher salt. When samples are prepared with pipette mixing (i.e., 0 s vortex mixing), flocs form at low salt only (Figure 2A). If instead samples are additionally subjected to 30 s vortex mixing, the majority of compositions form flocs (Figure 2B). In fact, adding even 1 s of vortex mixing to the sample preparation protocol significantly shifts the precipitate formation boundary. As the amount of vortex time is further increased in

increments of 1 s, the region of salt-polymer space in which at least one visible floc, or precipitate, forms after vortexing continues to expand to lower polyelectrolyte concentration. The shift in coacervate-precipitate boundary with various vortex durations is shown in Figure 2C. Visible flocs never form even after 30 seconds of vortex mixing at the highest tested salt concentration (4.5 M NaCl, just below the solubility limit of 5.4 M at 25°C⁷⁶) and at the lowest tested polyelectrolyte concentration (5 mM r.u.) with added salt. Thus, avoiding vortex-induced precipitation requires very high salt or low polyelectrolyte concentrations; otherwise, a longer vortex mixing duration results in aggregate formation.

2.2 Flow rate-dependent structure

To understand the mechanism of the vortex-induced aggregation in PAA-PAH PEC emulsions, we study the growth and aging of PECs in a microfluidic device at various volumetric flow rates (Q). Mixing in a microfluidic Y-junction enables precise control over the mixing mechanics and flow history, with mixing dominated by diffusion between PAA and PAH solutions across steady laminar streamlines. A schematic of the microfluidic device's mixing channel is shown in Figure 3A. Figure S2 provides the microfluidic mold SOLIDWORKS[®] design and a channel imaging schematic.

2.2.1 Droplet growth

To inform an eventual mechanism of vortex-induced aggregation between PEC coacervate droplets, we first seek to understand the dynamics of individual coacervate droplet growth in the microflu-

idic device. Here, we leverage microscopy to directly observe the size distribution of newly formed PEC-rich droplets once they reach the diffraction limit. The axial position (length l) along the mixing channel serves as an approximate proxy for the residence time τ in the diffusive mixing process. As droplets form near the channel's midplane, droplet size distributions are extracted from videos collected at constantly-spaced l , and used to produce the volume-averaged radius $\langle R \rangle$ at each l . Image processing and data analysis methodology is provided in ESI Note 3.1, including typical snapshots of droplets in flow (Figure S3); a visual summary of the algorithm to extract in-focus droplets from each video frame (Figure S4); and the measured droplet volume distributions and associated cumulative distribution functions used to find the mean radii for an example composition (Figure S5).

We find that PEC droplet growth is insensitive to the fluid flow rate in the tested Q -range. After an initial quick growth of the droplet radius past the resolution limit of the microscope, comparatively slow growth is observed (Figure S6A). Droplet sizes above the resolution limit emerge at an l_0 that depends on Q . A linear fit of l_0 versus Q gives an estimated timescale for initial droplet growth on the order of seconds (Figure S6B). The linear trend, i.e., that this timescale is Q -independent, suggests neither the shear rate nor the balance of convective and diffusive mixing within the microfluidic channel significantly affect initial droplet growth. Thus, it is unlikely that mechanisms of droplet formation and growth are able to explain the observed flow-induced formation of precipitate-like PEC flocs.

Once droplet size surpasses the microscope resolution limit, $\langle R \rangle$ remains $\sim 1 \mu\text{m}$ in the microfluidic device, due to the limited residence time. To monitor droplet size for a longer duration (~ 600 s) and assess the rate of droplet growth *after* the initial fast growth stage, we employed dynamic light scattering (DLS) (methodology in ESI Note 3.3). In DLS, the growth rate of $\langle R \rangle^3$ is linear in time after vortex mixing (Figure S7), consistent with growth dominated by Ostwald Ripening, i.e., diffusive transport of polyelectrolyte between PEC-rich droplets through the PEC-dilute phase.⁷⁷ The resulting growth rates in DLS are consistent with minimal on-chip growth beyond $\sim 1 \mu\text{m}$ (ESI Note 3.4).

The signature of fast initial growth followed by maintenance of $\langle R \rangle$ near $1 \mu\text{m}$ in the device is recovered over the range of salt and polyelectrolyte concentrations studied. Higher polyelectrolyte concentration appears to correlate with larger droplet size (Figure S8A). By contrast, at fixed polyelectrolyte concentration, the on-chip droplet growth rate is insensitive to NaCl concentration between 0 and 4.5 M (Figure S8B). Since polyelectrolyte properties are strongly salt-dependent, the latter observation is surprising, especially given the broad range of tested NaCl concentrations (with a solubility limit of 5.4 M⁷⁶). The growth rate of Ostwald ripening depends on solubility, molar volume, and surface tension of a soluble moiety—likely a polyanion-polycation pair in coacervation, as proposed by Veiss-Aranyi.⁷⁸ Further discussion of individual droplet growth is provided in ESI Note 3.5, including a possible mechanism that may reconcile salt-dependent properties and salt-independent drop growth. These observations merit deeper experimental exploration beyond the scope of this work. Herein, only the first few seconds of mixing matter, during which

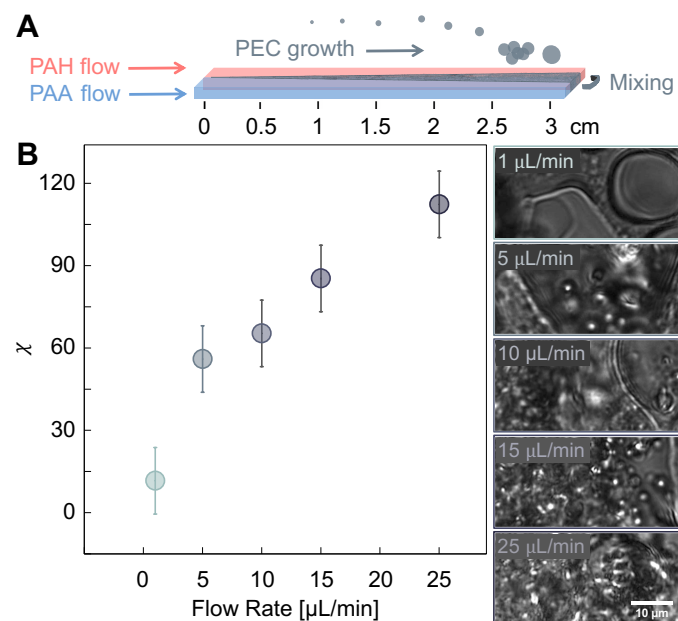


Fig. 3 Flow rate strongly controls PEC floc microstructure at flow-sensitive compositions (Figure 2). (A) PAA and PAH mix by diffusion in the mixing channel of a microfluidic Y-junction device; PECs form at the centerline, growing and sedimenting as residence time increases down the length of the channel. (B) PEC sediment microstructure increases in roughness, χ , when mixed at higher volumetric flow rate, Q , despite fixed composition (90 mM r.u. and 3 M NaCl). Associated snapshots show the PEC structure is smoother at low Q and more precipitate-like at high Q . Error bars represent standard deviation ($n = 3$).

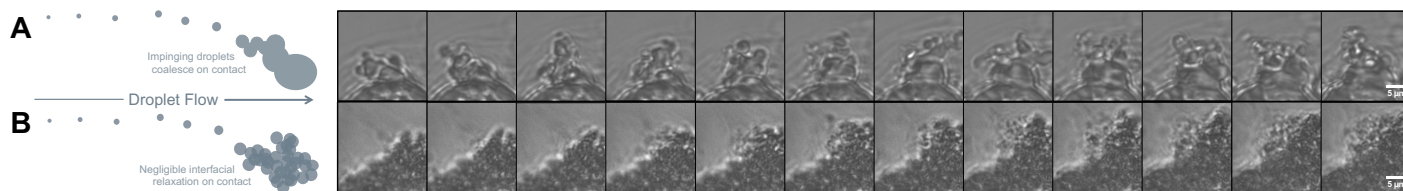


Fig. 4 Mechanism of droplet addition during PEC growth controls its microstructure. (A) Time series of growth by direct coalescence of droplets onto PEC sediment results in a smooth, coacervate microstructure. (B) Time series of growth by addition of droplets in quick succession (higher Q at fixed composition, or lower NaCl at fixed Q) results in negligible interfacial relaxation during droplet addition and an aggregated, precipitate microstructure.

(R) $\sim 1 \mu\text{m}$ over the range of conditions studied, enabling comparison of flow-induced PEC floc formation across compositions.

2.2.2 Dynamics of PEC floc growth

By contrast to droplet growth, the morphology and microscale roughness of PEC sediment (as observed at the bottom of the microfluidic channel) is strongly dependent on Q . At a given concentration within the region of sensitivity to vortex-induced aggregation (Figure 2), increases in Q induce a more roughly aggregated PEC sediment in microfluidics. We quantify the structural sensitivity to flow rate using the Euler parameter (χ) (ESI Note 4.1) extracted from thresholded, despeckled images of PEC sediment in the microfluidic channel (Figure S9). Spatial non-uniformity, time-dependence, and lack of scaling hierarchy prevent a fractal description typically used for colloidal aggregation processes. χ is a common topological characteristic in mathematics. Here χ refers to the number of noncontiguous regions within each binarized snapshot of the aggregate.[†] Sediments with more abundant internal interfaces (i.e., a greater precipitate character) will have more frequent contrast variation in brightfield microscopy, and thus larger values of χ . The average χ of PEC sediments increases monotonically with increasing Q (Figure 3B). These results demonstrate that the non-equilibrium PEC microstructure depends on the strength of the laminar mixing flow.

To gain better mechanistic insight into this flow rate-dependent roughness, we directly observe the mechanism of coacervated vs. precipitated PEC sediment growth in the microfluidic channel. PEC sediments that grow by a mechanism of individual droplets coalescing directly to the sediment retain a smooth microstructure (Figure 4A). By contrast, aggregated PEC microstructures form when individual droplets irreversibly adhere to existing aggregates and retain their shape as the sediment grows (Figure 4B). As flow rate is increased during laminar microfluidic mixing of PAA and PAH salt solutions at flow-sensitive compositions, PEC sediment growth shifts between these mechanisms, respectively forming PECs with smooth or aggregated microstructures.

In light of these observations, we deduce that PAA-PAH precipitates reported by us and others^{57,59} must be flow-induced flocculates of *partially-coalesced coacervate droplets*, rather than aggregates of solid particles. Since flow can toggle a transition in growth mechanism at fixed composition—i.e., without altering the PEC-rich phase rheology, which maintains $G'' > G'$ even

at 0 M NaCl (Figure S10)—coalescence should also occur during formation of precipitated sediments. Merely, when PEC sediment growth occurs without time for relaxation of the liquid bridge between newly-adhered droplets and the sediment prior to addition of the next droplet, a "precipitate" forms: the liquid bridges persist, leading to a floc-like precipitate structure.

To summarize, conditions favoring complete coalescence of PEC-rich droplets always produce coacervate emulsions at the earliest observable times. Meanwhile, partial coalescence always produces flocculated, aggregate or "precipitate" structures at early times. The finding that PAA-PAH precipitates are actually composed of partially-coalesced coacervate droplets is further supported by observations to be described later. In particular, partial coalescence of aggregating droplets as the mechanistic origin of PEC precipitate morphologies suggests that PEC-dilute phase gets trapped in the interstitial space between droplets as they adhere to the growing PEC. Further, ongoing interfacial relaxation of these partially-coalesced structures should result in time-dependent smoothening of the aggregates. Observations of aggregate relaxation and dilute-phase inclusions are discussed in the sections to follow.

2.3 Concentration-dependent structure

While the mixing flow conditions determine the microstructure of PECs at fixed salt and polymer composition, the composition determines whether coalescence or aggregation is the mechanism of addition to the structure for fixed flow conditions. Microfluidic mixing of PAA and PAH salt solutions at $Q = 25 \mu\text{L}/\text{min}$ reveals that PECs grow by coalescence at high NaCl and low electrolyte concentration, resulting in a smooth coacervate microstructure at these conditions (Figure S11A). Elsewhere, the PECs grow by droplet aggregation and, thus, precipitate microstructures form. Despite the different flow mixing approach, the microfluidic precipitate boundary at $25 \mu\text{L}/\text{min}$ (Figure S11B) is similar to the boundary for obtained by visual inspection for vortex-induced flocculate formation ($> 10\text{s}$ of μm) after 1 s vortex (Figure 2).

For all mixing flow conditions, the aggregation propensity decreases with salt and increases with total polymer concentration, as observed in pipette and vortex mixing (Figure 2) and microfluidics (Figure S11). Figure 5 shows PAA-PAH emulsion samples that were settled quiescently for 48 hours in a glass-bottomed 96-well plate prior to observation, i.e. PECs formed under a fourth flow mixing condition. The microstructural roughness of these samples also qualitatively increases toward higher polymer con-

[†] Thus, χ depends on crop size, but can be compared if crop size within the sediment is fixed across either samples (Figure 3) or timescales (Figure 6).

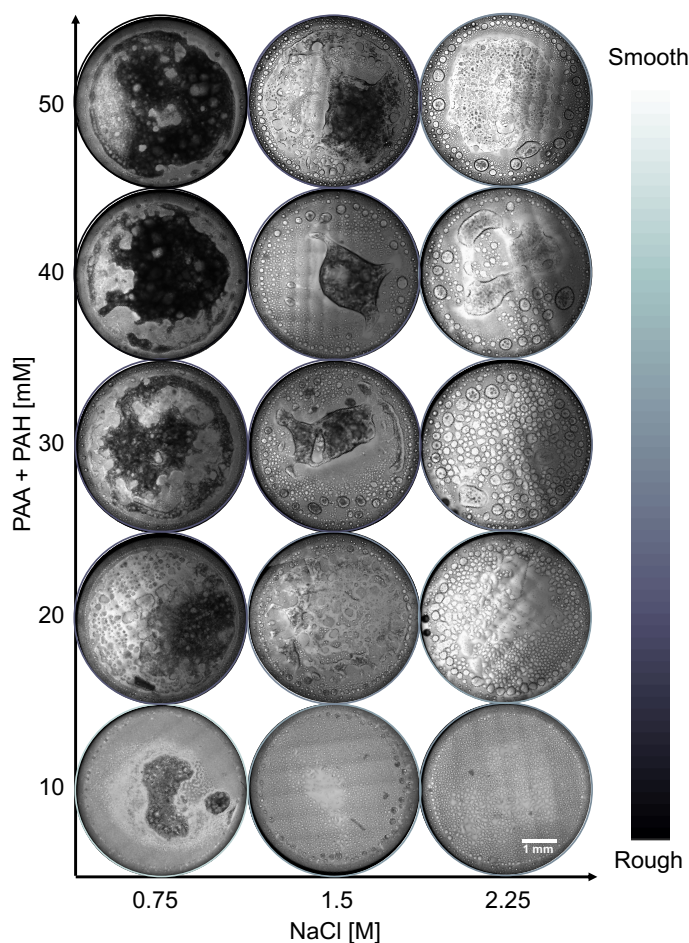


Fig. 5 Microstructural roughness increases as a function of total polyelectrolyte concentration and decreases as a function of salt. Tiled micrographs of PEC sediment, grown via gravitational sedimentation of PEC emulsion in a 96-well plate, were imaged at 48 hours. Roughness is qualitatively color-coded using the fraction of translucent pixels in the well (see ESI Note 4.4 and Figure S13 for calculation details).

centration and lower salt concentration, as shown at a broader range of compositions in Figure S13. Consistency across markedly different flow histories suggests that the generality of this trend across mixing methods.

2.4 Time-dependent structure

We observe microstructural aging of aggregated PEC condensates that occurs in two stages. The first, which occurs within minutes, involves the interfacial coarsening of micron-scale aggregates from relatively rough to relatively smooth structures. The second is characterized by the slow coarsening of dilute-phase inclusions within the dense PEC and occurs over days to weeks.

During the initial stage (Figure 6), the microstructural roughness of all PEC aggregates observed decreases exponentially with time constant τ_{relax} . This relaxation can be quantified by the decrease in χ . Here χ is independent of how micrographs are cropped around the aggregate and unaffected by ongoing sedimentation nearby. τ_{relax} is extracted from the χ data at times before the precipitate area changes < 2% in 90 s to avoid skew

from the relaxed microstructure. Image processing, video analysis, and fitting protocols are described in further detail in ESI Note 5.2.

Micrographs of an example PEC aggregate relaxing and the associated relaxation fit are shown in Figure 6AB. That an exponential fit describes the relaxation, with no trend in the extracted time constants τ_{relax} as a function of initial aggregate size (Figure S17) indicates a scale-invariant relaxation rate. This suggests that the aggregates have a self-similar morphology over a range of length scales at least within the observed micron-scale imaging range.

τ_{relax} is sensitive to the vortex mixing duration across samples at a variety of compositions with statistical significance (Pearson correlation coefficient $r = -0.39$ and two-tailed hypothesis $p = 0.014$), suggesting that precipitates prepared with increasing mixing strength are more likely to relax quickly. This negative correlation is readily apparent in Figure 6B, which shows average values of τ_{relax} at various compositions and vortex mixing durations. Except for vortex mixing time, τ_{relax} is uncorrelated to nearly all other variables such as initial aggregate size (S), the S -normalized initial χ , the dispersity in τ_{relax} for different structures, and the start-time of the relaxation video (~ 2.5 min after mixing) (Figure S17). Therefore, none of these experimental factors can account for the dependence of aggregate relaxation on vortex time.

Intriguingly, τ_{relax} is also insensitive to the PEC composition (Figure S17). By contrast, the viscoelastic moduli of the PAA-PAH dense phase decrease slightly with polymer concentration⁷⁹ and strongly with salt. Lack of correlation between τ_{relax} and either salt or polyelectrolyte concentration suggests that the relaxation behavior of PEC aggregates *cannot* be solely determined by its equilibrium rheology. In further support of this result, the extracted timescale for aggregate relaxation is order $\tau_{relax} \sim 100$ s, whereas the longest viscoelastic relaxation time for the PAA-PAH system at 30 mM r.u. and 0 M NaCl is $\tau_{rheol} \sim 10$ s (extrapolated from the time-ionic strength superposition at comparable molecular weight,⁷⁹ see ESI Note 5.3). τ_{relax} therefore exceeds τ_{rheol} by an order of magnitude, suggesting that elastic stresses within the dense phase are able to relax within the aggregate relaxation time. A potential explanation for this is proposed in the Discussion, where other timescales that may be important are also considered.

The second stage of coarsening occurs after the PEC condensate roughness tracked in Figure 6 will have already relaxed, such as by Day 2 after mixing (Figure 5). Even though aggregates form in microfluidics at some compositions in Figure 5, their roughness does not originate from aggregated droplet structures. Fluorescent carboxylated polystyrene tracer particles—which selectively partition into the PAA-PAH PEC dense phase²⁶—reveal spherical dilute-phase inclusions trapped within the dense phase sediment (Figure S14). The inclusions range from 10 - 100s μm in size and remain trapped by high viscosity contrast and low surface tension (low Laplace pressure). In prior work, we observed coarsening of dilute inclusions for over 2.5 weeks at 100 mM r.u. and 0 M NaCl.²⁶ Here, we demonstrate that significant coarsening of dilute-phase inclusions occurs at many compositions in gravitationally-sedimented samples after 10 days, including at high ionic strength (3.75 M NaCl) (Figure S15). Microstructural

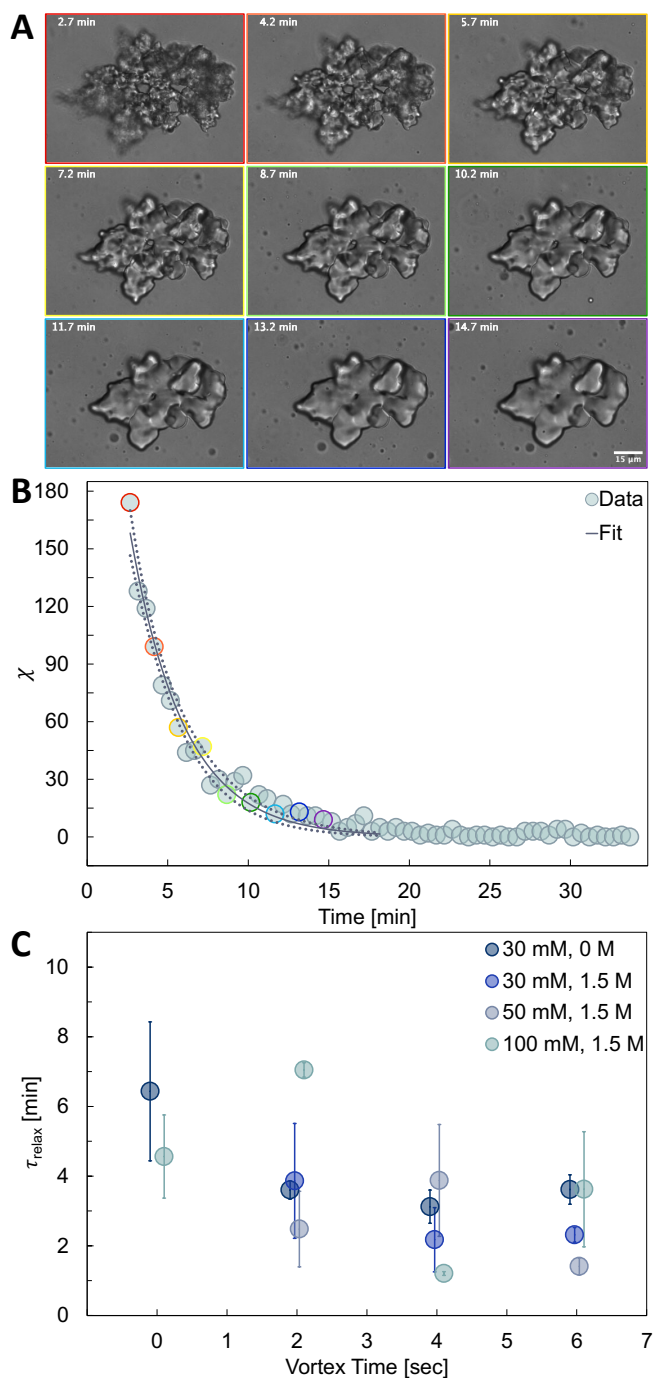


Fig. 6 Time-dependent aging of PEC structure. (A) Relaxation of a typical aggregate, with associated exponential fit and micrographs at various times (30 mM r.u. and 0 M NaCl, 2 s vortex mixing). (B) Two parameter exponential fit of Euler characteristic, χ , during the aggregate relaxation over times for which its area changes $> 2\%$ in 90 s, as $b_1 e^{-t/b_2}$. Dotted lines represent 95% confidence interval of the fit. (C) Aggregate relaxation time constants, $\tau_{relax} = \frac{1}{b_2}$, are extracted from the exponential fits and plotted to illustrate the statistically significant ($p = 0.01$) correlation between τ_{relax} and vortex time at a variety of compositions (see ESI Figure S17). Error bars represent a combination of regression uncertainty based on the standard error of the fit and replicate uncertainty based on the number of structures analyzed (typically $n = 3$).

roughness decreases commensurately (Figure S16).

Thus, coarsening of dilute-phase inclusions can prevent mm-scale PEC condensates from achieving equilibrium across composition space for weeks after initial LLPS. Two possible mechanisms can account for inclusion formation. One explanation is that PEC condensate droplets form at a nonequilibrium *composition*, then continue equilibrating after sedimentation to form spontaneous inclusions within the condensate. Measurements showing that coacervate phase boundaries take as long as 90 minutes to equilibrate after poor mixing support this possibility.³⁵ Another possibility is that dilute phase becomes trapped in the interstices between droplets during aggregate growth (Figure 4B). As the liquid bridges continue to relax while the inclusions coarsen, an aggregate-free sediment containing dilute inclusions forms. We leave a more in-depth characterization of the formation and coarsening of dilute-phase inclusions to further study.

3 Discussion

3.1 Precipitates: Colloidal aggregates of liquid PEC droplets

We have observed flow-induced floc-like PEC aggregates in the PAA-PAH system over a wide range of compositions. Using classifications established by a consensus of prior literature based on micron-scale PEC structure,^{57–63} one could call these “precipitates,” which might imply that they are composed of microscopic solids or have solid-like rheology at equilibrium.^{20–22,51–56} Instead, we find that “precipitates” of PAA-PAH comprise aggregates of viscoelastic liquid-like colloidal PEC coacervate droplets, and they coexist with smaller spherical droplets. They form by aggregation of these individual coacervate droplets as observed directly in microfluidics, and they grow and relax by coarsening processes consistent with a sticky Rouse-like viscoelastic fluid. Further, the equilibrium rheology of the PAA-PAH PEC dense phase is loss-modulus dominant even at compositions that form aggregates.

The aggregates also relax into a smooth microstructure over time. The characteristic age time τ_{relax} of the PEC aggregates is two orders of magnitude longer than the associated viscoelastic relaxation timescale τ_{rheol} , suggesting that the properties of PEC aggregates cannot be predicted by the equilibrium viscoelasticity alone. In fact, PAA-PAH PEC aggregates have a higher propensity to form at higher total polyelectrolyte concentration, whereas the dense-phase moduli decrease with polyelectrolyte concentration at equilibrium.⁷⁹ These observations are consistent with the idea that PAA-PAH PEC “precipitates” with micron-scale features do not comprise molecular-scale solids.

3.2 Mechanism of “precipitate” formation

3.2.1 The importance of colloidal transport

Broadly, our results demonstrate that the imposed flow during mixing can be used to control micron-scale PEC morphology without modifying the chemistry or composition. In microfluidics, we find that the non-equilibrium condensate microstructure—and even whether or not aggregates form at a given composition—depends on the strength of the laminar mixing flow. Thus, our observations suggest that the micron-scale colloidal transport of PEC droplets themselves is critical to understanding and controlling “precipitate” formation.

3.2.2 "Precipitate" formation as flow-enhanced aggregation of PEC coacervate emulsions

Our observations are consistent with a hypothesis whereby PAA-PAH PEC "precipitates" grow by flow-enhanced aggregation of PEC-rich coacervate droplets. Briefly, flow-enhanced aggregation of colloidal suspensions can occur when velocity gradients in a flow (or relative velocities between particles due to acceleration or non-vanishing droplet Reynolds number, Re_d) enhance the rate of encounters and collisions between colloidal particles.^{68,69} Existing theories for flow-enhanced aggregation involve extensions of the Smoluchowski theory of colloidal instability, whereby growth of colloidal aggregates occurs as a convection-diffusion reaction process, with aggregates of a particular size representing the reacting species.^{68,80} In this framework, the "reaction" rate between individual droplets and droplet clusters that produces aggregates depends on both the characteristic time scale over which droplets encounter and collide with each other (or larger aggregates) by colloidal transport processes—i.e., τ_{imp} —as well as the probability with which such encounters lead to binding between individual droplets (or droplet clusters) and larger aggregates. We expect that the time scale of collisions will depend both on the details of the flow and the volume fraction of droplets, ϕ_d . In PAA-PAH PEC growth, we experimentally observe that droplet collisions always leads to binding.

In models of flow-enhanced aggregation, increases in shear rate lead to an increase in the rate of pair encounters between droplets and aggregates. This increases the overall aggregate formation rate.⁶⁸ The key parameter in models that govern flow-enhanced aggregation is the droplet Péclet number, Pe_d . In the case of PAA-PAH PECs, we observe that higher flow and shear rates favor the formation of "precipitates," consistent with the expectation that increased Re_d and Pe_d increase τ_{imp} and aggregate formation.

At the droplet scale, we observe a coacervate-to-aggregate transition induced by increased mixing intensity (e.g., from pipette to vortex mixing), i.e., by increasing Re_d and Pe_d . (Estimates of Re_d and Pe_d in the various flow environments for a typical PEC droplet are reported in ESI Note 6.) Flow rate-dependent results in microfluidics demonstrate that the same effect can be achieved even at relatively small Re_d , when viscous effects remain comparable to inertial effects on the droplets in flow. In microfluidics, droplet Re_d only ranges from 0.035 to 1.74, yet a composition-dependent aggregation transition is still observed. Whereas growing colloidal droplets and aggregates both remain entrained in the flow during pipette and vortex mixing, aggregates grow on static sediment in microfluidics. Increasing the microfluidic flow rate from 0.2 to 25 $\mu\text{L}/\text{min}$ corresponds to an increase from 500 to 25000 $\mu\text{m}/\text{sec}$ in the average linear flow rate of droplets, thereby increasing their velocity on encountering the sediment, while simultaneously decreasing the time between successive droplet impacts, τ_{imp} . In further support of the flow-enhanced aggregation hypothesis, τ_{imp} greatly increases and impact velocity decreases as soon as a PEC suspension is accelerated on the vortex mixer (i.e., within 1 second of vortex mixing), by which time a shift in precipitate formation is already observed. Additionally, at fixed flow conditions, we observe that compositions with a larger ϕ_d (i.e.,

increasing r.u. at fixed salt, decreasing salt at fixed r.u.) favor "precipitate" formation, consistent with the fact that increasing ϕ_d decreases τ_{imp} , with all else constant. These observations overwhelmingly support a flow-enhanced aggregation mechanism.

An unresolved question regarding our hypothesis—namely, that PAA-PAH "precipitates" form by flow-enhanced colloidal aggregation of PEC-rich droplets—is the origin of colloidal attraction between droplets suspended in the PEC-dilute phase: in many systems, droplet collisions do not necessarily lead to binding or aggregation. In the case of PAA-PAH PECs, possibilities could include van der Waals-type interactions, or potentially depletion-like interactions from either dilute-phase polyelectrolytes or polyelectrolyte pairs. Regardless of their origin, it is not clear why colloidal attractions between droplets would result in aggregates only under flows with sufficient velocity and shear rate (and smooth coacervates elsewhere); this transition is not a common feature of flow-enhanced aggregation models. One possibility is that a significant energetic barrier to aggregation exists that can be overcome only by sufficiently strong hydrodynamic forces in the coacervate suspension. A possible source of such a barrier could be long-range repulsive interactions between droplets, caused either by sufficient excess surface charge of the droplets, or by steric interactions between dangling polyelectrolyte tails at the droplet surface. However, a strong energetic barrier seems at odds with our observations that droplet collisions always lead to coalescence, even at low Re_d and in quiescent systems. Another possibility is that viscoelasticity of the PEC droplets results in different behavior when colliding under different flow conditions. Flows that produce precipitate structures could cause deformation of coacervate chains within droplets, forming nanoscale flow-dependent structures that might alter the nonlinear rheology of the coacervate, and thus possibly leading to rheologically-frustrated states that do not form quiescently. A molecular-level study of flow-induced structuring of coacervates and its connection to nonlinear rheology would be an interesting direction for future study. Droplet viscoelasticity and morphology are not commonly considered in flow-enhanced aggregation models, which typically assume solid and spherical particles. We hope this discussion will inspire future studies that more thoroughly investigate the colloidal interactions between suspended coacervate droplets, including their molecular underpinnings and any influence of flow and non-equilibrium droplet rheology.

3.3 Aging of aggregated structures

Our experiments clearly show that the "precipitates" observed in the PAA-PAH system are not static structures. Rather, they exhibit aging characteristic of colloidal structures comprised of sticky rouse fluid. Specifically, observations of "precipitate" aging reveal several key features that are common to the interfacial coarsening of viscoelastic liquid emulsions. Aggregated structures coarsen toward progressively lower surface area structures (indicated here by a decrease in the Euler characteristic), consistent with interfacially-driven coarsening. The short-time kinetics of interfacial coarsening exhibit an exponential time-dependence, with a characteristic time scale τ_{relax} that is insensitive to the

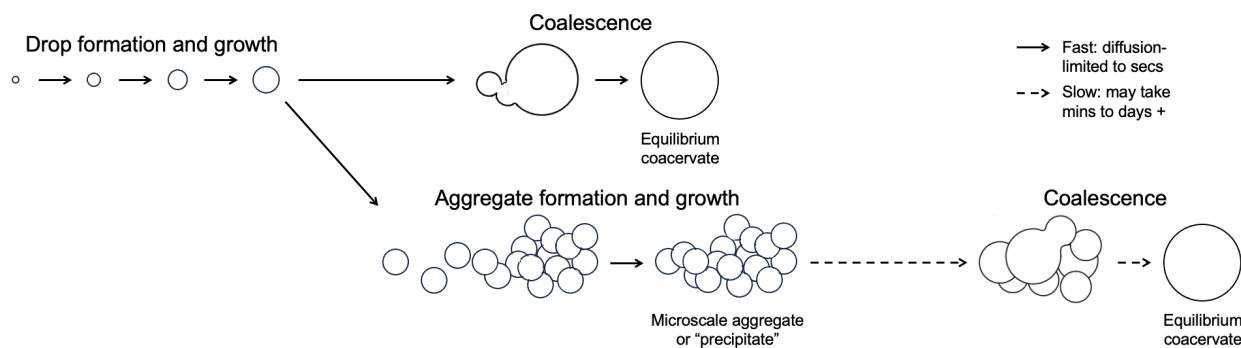


Fig. 7 Mechanism of growth and aging from mixed polyanion and polycation solutions. PEC droplets quickly form, then either: (1) directly coalesce into a smooth microstructure and equilibrium viscoelastic liquid; or (2) form an intermediate aggregated state, which can relax into near-equilibrium droplets or persist as a kinetically-trapped precipitate over observable timescales. Which path is taken depends on the rheology and interfacial properties of the droplets; the macroion chemistry; and the mixing conditions, which highlights the importance of mass transport and colloidal effects in PEC formation.

size of the aggregated structure. This is consistent with both experiments and theoretical models of capillary thinning of viscoelastic polymer solutions, in which the interfacial bridge diameter between droplets during pinch-off decays exponentially in time.⁸¹ Drop pinch-off is the better-studied complement to coalescence, which is poorly studied especially for viscoelastic systems.⁸² Broadly, viscoelastic droplet coalescence is known to proceed according to a series of processes with distinct physics, and therefore distinct scaling behavior. This sequence is known to involve at minimum: (1) viscous-dominated drainage of the liquid film between droplets during approach; (2) inertio-capillary flow that governs the initial formation of a liquid bridge; (3) visco-capillary flow that resists the growth of the liquid bridge; and (4) bulk viscoelastic relaxation which dominates the flow inside droplets during coalescence. Thus, coarsening of droplets is a complicated process with many physical timescales that may be important.

Our initial comparison of τ_{relax} , the characteristic timescale of exponential aging extracted from aggregate relaxation experiments (see Section 2.4), is not consistent with the expected time scales for these processes. τ_{relax} (typically minutes) is an order of magnitude slower than the measured longest viscoelastic relaxation time of the PEC-dense phase, τ_{rheol} (around 10 s, see ESI Note 5.3). Additionally, aggregate relaxation is not dominated by initial coalescence events or inertio- or visco-capillarity. The visco-capillary time $\tau_{vc} = \frac{\mu R}{\gamma}$ (where μ is viscosity, R is the average drop size, and γ is the surface tension), sets the rate of interfacial relaxation in situations where density has a negligible effect but both capillary and viscous forces are important (e.g., coalescence of viscous fluids). When inertia predominates over viscous effects (e.g., during drop pinch-off), the inertio-capillary time, $\tau_{ic} = \sqrt{\frac{\rho R^3}{\gamma}}$ (where ρ is the density), becomes relevant.⁸³ Here, τ_{vc} is of order 1 ms, and $\tau_{ic} \sim 10^{-7}$ s (ESI Note 5.3). $\tau_{relax} \sim 100$ s thus exceeds τ_{vc} and τ_{ic} by more than 5 orders of magnitude. Thus, the observed aggregate relaxation extends well past the time scales associated with coalescence, viscoelastic relaxation, or visco- or inertio-capillarity. That τ_{relax} is a similar magnitude to τ_{rheol} suggests that viscoelastic relaxation is part of the coalescence problem dominating the aging dynamics, but does not

alone provide a complete explanation.

Instead, we propose that such slow relaxation may be consistent with elasto-capillary coalescence, i.e. relaxation after viscoelastic coalescence in which elasticity plays an important role. Describing relaxation by elasto-capillary coalescence is an active area of study with conflicting models and findings proposed, using aqueous PEO solutions. Dekker et al. found that elasticity does not affect relaxation rates after coalescence by observing the temporal evolution of a bridge between spreading droplets.⁸² Others argue that while kinematic similarity is retained between coalescence, spreading, and drop pinch-off, dynamic similarity between the three is affected by the presence of elasticity.⁸⁴ In general, the relationship between droplet radius and the time-evolution of the neck in the case of elasto-capillary coalescence in various geometries is not established. However, Varma et al.⁸⁴ develop regimes of dimensionless $\tau^* = \sqrt{\frac{Oh \tau_{rheol}}{\tau_{ic}}}$ (calculation in ESI Note 5.3.1), where Oh is the Ohnesorge number, to denote where inertio-elastic, visco-elastic, or elastic effects dominate the coalescence relaxation. $\tau^* \approx 8.1 \times 10^5$ for our system, suggesting that the relaxation is strongly elasticity-dominated (for aqueous PEO, elasticity dominates above $\tau^* \approx 100$). Though the chemistry and rheology are certainly different between PEO solutions and coacervates, in our view elasticity-dominated coalescence is the most likely explanation for the extremely slow relaxation of PEC aggregates after coalescence.

We anticipate that the present study will motivate further experimental work toward understanding the conditions of material properties and fluid physics under which elasto-capillary dominated behavior is expected to govern the coalescence of viscoelastic droplet suspensions. In this regard, PEC aggregates themselves may be excellent candidate materials for understanding viscoelastic coalescence relaxation fundamentally, as their viscoelastic rheology and very low surface tension lead to long time scales over which coalescence can be observed.

3.4 Summary: PEC growth, aging, and aggregate prevalence

The mechanism of PEC precipitate growth and aging in coacervate emulsions is summarized in Figure 7. As PEC-rich droplets

form during mixing, they grow by a competition of coalescence to form smooth condensates, and flow-enhanced aggregation to form rough, precipitate-like flocs. Whether a precipitate or smooth coacervate forms at a given length scale is thus determined by the balance between: (1) the characteristic time scale τ_{imp} between successive collisions between droplets or droplet aggregates, and (2) the characteristic time τ_{relax} of viscoelastic relaxation after droplet coalescence. These two processes—precipitate growth through droplet collision and relaxation through interfacial coarsening—can occur simultaneously. If τ_{imp} is large enough relative to coalescence relaxation, then structure formation is dominated by coalescence and a smooth coacervate forms. Conversely, if τ_{imp} is small enough, flow-enhanced aggregation of droplets is too fast for interfacial coarsening to occur, flow-induced aggregation is observed, and an aggregated "precipitate" is observed at early sample ages. According to theories of flow-enhanced colloidal aggregation, this balance will be controlled by the volume fraction of droplets ϕ_d as well as the mixing flow intensity represented by Re_d and Pe_d . Meanwhile, the rheology and size of individual PEC-rich droplets control the time scale over which droplet aggregates persist before interfacial relaxation. Precipitates signified by solid-like rheology ($G' > G''$ at measurably low frequencies) are arrested at the molecular scale and should hence resist microstructural aging over observable timescales. Using microrheology or microscopy-based aging studies, such precipitates can be distinguished from the colloidal aggregates of viscoelastic liquid droplets herein that interfacially coarsen. We propose herein that this relaxation process occurs in two stages: (1) elastic-dominated coalescence of the viscoelastic droplets, with a time scale τ^* of order seconds to hours depending on droplet rheology and surface properties; and (2) slow, viscous-dominated coarsening of any dilute-phase inclusions trapped within larger PEC aggregates during the initial coarsening stage, which can take days to months.²⁶

We posit that "precipitates"—namely, the colloidal aggregates of PEC-rich droplets we observe here—are prevalent in PEC-forming systems due to a confluence of factors unique to PEC-based materials that can lead to their stabilization. With relatively large dense-phase viscosities and viscoelasticity, low interfacial tension, and a large viscosity ratio between the dense and dilute phases, we surmise that PEC droplet aggregates have very slow time scales of interfacial coarsening (10s of minutes or longer) and are particularly facile at trapping dilute phase inclusions. When the aggregate size is increased from microns to millimeters, PECs can take more than several weeks to completely coarsen into spherical droplets. Common steps in PEC preparation like vortex mixing can also induce aggregation, further increasing the prevalence of the precipitate microstructures reported in the literature.

These factors apply even in chemistries such as the PAA-PAH system studied in this work, where the constituent droplets themselves are slow-flowing viscoelastic liquids. In other chemistries, longer chain lengths, or lower temperatures where the bulk PEC has G' -dominant rheology, the micron-scale PEC aggregate theoretically could be made up of solid particles, resulting in an infinite persistence time and unchanging microstructure. Since solid particles cannot undergo classical liquid coarsening mech-

anisms, then the associated length scale of aggregated constituents should be much smaller than order $(R) \approx 1 \mu\text{m}$, at a length scale where local polyelectrolyte dynamics become arrested. Literature on solid-like PECs is consistent with this extension of our mechanistic understanding: a recent study of solid-like poly[(vinylbenzyl)trimethylammonium chloride]/poly[sodium 4-styrenesulfonate] PECs find "cobble stones" at 1-3 nm in cryo-TEM, suggesting "formation of local aggregations of polyelectrolyte chains."⁶² Thus, our work is consistent with the idea that micron-scale PEC aggregates of any chemistry must be partially crystalline or glassy if they persist long term (i.e., true rheological precipitates); whereas all intrinsically-disordered, two-polyelectrolyte PEC aggregates eventually relax and are not rheologically solid-like.

Future studies should take into account the strong sensitivity of colloidal aggregation in coacervate-forming PECs to the flow conditions encountered during their formation and processing. Our findings suggest that mixing flows can be manipulated to either suppress or enhance PEC aggregate formation as desired, regardless of the initial or final fluid compositions. This is particularly important when considering the scalability of processes to produce PEC materials, as the details of flow can change considerably with the scale of processing equipment. For example, given that millimeter-scale PEC structures can take at least several weeks to relax, the scale-up of a process used to produce PEC-based materials cannot result in a uniform, single-phase material unless aggregation-related issues and the associated dilute phase entrapment are overcome.

Furthermore, we urge researchers to consider the possible impacts of aggregate formation, relaxation, and dilute phase entrapment on rheological measurements of the PEC dense phase. The apparent rheology of a PEC condensate prepared via centrifugation reflects the rheological response of a dense phase containing entrapped dilute phase,²⁶ since classical protocols result in measuring an "opaque white" PEC-rich dense phase.⁷⁹ In the same vein, our prior observation that aged and newly-mixed PAA-PAH condensates have similar viscosity²⁶ might be attributable to the very high ionic strength (4.5 M NaCl), where neither PEC condensate aggregates nor dilute inclusions are observed.

4 Conclusions

Tuning the flow conditions of mixing enables polyelectrolyte condensate droplets to form aggregated microstructures characteristic of "precipitates". Specifically, PEC condensate growth can be toggled between droplet coalescence (to form smooth coacervates) and flow-enhanced aggregation (to form a precipitate) not only by changing composition—which controls both droplet rheology and concentration—but also by changing mixing parameters that affect the relative flow rates and collision frequencies between PEC droplets. In short, the condensate coarsening mechanism depends sensitively on both the processing flow and PEC rheology. Flows with higher strain rates and longer residence times result in an aggregated PEC structure when the time scale for droplet collisions is much faster than the time scale(s) of droplet coalescence. This behavior is favored at low ionic strength and high polyelectrolyte concentrations, which accom-

pany increased volume fraction, viscosity, and elasticity of the PEC-dense phase. Such aggregation is surprisingly easy to induce, suggesting that the conventional concept of a composition state diagram with distinct precipitate and coacervate regions must be updated to account for the effects of mixing and processing flows.

We further demonstrate that PEC aggregates need not be static structures. In fact, all flow-induced aggregates we observe in the PAA-PAH system, including some previously characterized as precipitate,^{57,59} eventually exhibit interfacial coarsening and relaxation. Characteristic timescale analysis suggest this relaxation is not controlled by molecular-level relaxation, but rather by a very slow process involving elasticity-dominated coalescence of droplets despite their overall viscous-dominated rheology. PAA-PAH PEC aggregates follow an exponential relaxation rate, with a characteristic time scale that correlates with vortex mixing time, again highlighting the influence of processing parameters on the condensate microstructure. Additionally, in larger (mm-scale) PECs formed from gravitational settling, we observe that trapped dilute inclusions in the PEC sediment slowly coarsen for weeks or more, even at high ionic strength, suggesting that complete equilibration of the microstructure—and possibly composition—is never achieved during this time.

Our work supports the idea that microstructural and nanoscale precipitation are wholly separate effects mechanistically. While rheologically-solid PECs are kinetically arrested at the molecular level, microscale aggregated PECs are not. Going forward, we suggest that the term "precipitate" be used solely to describe PECs for which bulk rheology measurements reveal molecular-level arrest, in order to distinguish their morphology, structure, and behavior from PEC droplet aggregates like those described herein, with the understanding that the latter are slowly-relaxing and their formation depends on mixing parameters like flow. Overall, our results suggest that, to gain control over PEC behavior out of equilibrium, it will be critical to further understand: (1) the initial kinetics of LLPS and droplet growth and its interplay with mixing parameters as we have begun in this work; (2) colloidal interactions between PEC droplets and their influence on flow-enhanced droplet aggregation; (3) the structure and time-dependent rheology of PEC droplet aggregates at multiple length scales (from individual droplets to their assemblies). Such studies will open the door to manipulating PECs orthogonally to chemistry, and to controlling their formation and non-equilibrium structure.

5 Experimental Methods

5.1 Materials

Poly(allylamine hydrochloride) (PAH) is used as the polycation and poly(acrylic acid sodium salt) (PAA) as the polyanion for the present studies. Both polyelectrolytes are purchased from Sigma-Aldrich and used without further purification. PAH has $M_w = 17,500 \text{ g mol}^{-1}$, corresponding to an average degree of polymerization $N = 187$ as dried powder. PAA has $M_w = 15,000 \text{ g mol}^{-1}$, corresponding to $N = 160$ as 35 wt% solution. Sodium chloride (NaCl, $\geq 99\%$) is purchased from Spectrum Chemical and used as received. Milli-Q water is generated by purifying deionized water using a Millipore Sigma Simplicity[®] UV system, achieving a resis-

tivity of $18.2 \text{ M}\Omega\text{-cm}$ (25°C) prior to use. We select the PAA-PAH pair for our study due to significant past efforts to characterize its equilibrium state behavior^{18,26,57,59} and rheology.^{24,26,79}

5.2 Preparation of stock solutions

Prior to mixing, a stock solution of each polyelectrolyte is prepared in Milli-Q water at a concentration of 1 M with respect to the number of repeat units (r.u.). PAH powder is dried at elevated temperature in a vacuum oven for at least 4 hours prior to preparing its stock gravimetrically. PAA stock is prepared volumetrically using a density of 1.25 g mL^{-1} (25°C) as provided by the manufacturer. In addition, a 5 M NaCl stock is prepared gravimetrically. Stocks are stirred until they are transparent. We find no evidence of salting-out of the PAA or self-assembly of PAH prior to the mixing of the two polyelectrolyte solutions, as confirmed by turbidity measurement and DLS of the individual stock solutions.

5.3 Mixing and flow conditions

Aqueous solutions of polyelectrolyte and added NaCl are prepared by diluting the stock solutions such that the final mixtures have a 1:1 r.u. ratio of polyacid:polybase groups. Since PAH and PAA each have pKa comparably spaced from neutrality,⁶⁶ the final mixed pH was measured to be ~ 6.5 . Thus, pH adjustment prior to mixing is unnecessary, enabling precise equivalence of Na^+ and Cl^- ions and chain-bound acid/base groups, as well as near-complete ionization of polyelectrolytes at the final pH.^{18,79}

5.3.1 Microfluidic mixing

Microfluidic mixing in a Y-junction geometry was used to study the effects of steady laminar flows on PEC formation and aging. Details of the device geometry and fabrication are available in Note 1, ESI. In microfluidic mixing experiments, solutions of PAA and PAH were individually diluted from the stock solutions to the final post-mixing salt and total r.u. concentration. Each solution was loaded into a 5 mL syringe, capped with a 23-gauge McMaster-Carr stainless steel dispensing needle, connected to Tygon[®] ND-100-80 tubing with 0.51 mm inner diameter, and loaded onto a New Era SyringeTwo (NE-4000) programmable syringe pump. The two-channel pump minimizes transient differences in flow rate to ensure 1:1 mixing of the two precursor solutions. Next, the tubing was inserted into the cured polydimethylsiloxane (PDMS) upper layer of a microfluidic chip with Y-junction mixing channel and flow was turned on. Variation of the mixing channel dimensions (width $432 \pm 8 \mu\text{m}$ and height $38 \pm 3 \mu\text{m}$) remains below $\sim 1\%$ throughout the channel length as measured by profilometry of the 3D-printed negative master using a Keyence VHX-5000 digital microscope.

At least 15 minutes of flow rate stabilization (4.6 chip volumes at the slowest flow rate) to reach steady state was allowed prior to initiating observations of droplets in flow, sediment morphology, and/or the droplet addition mechanism. Minimizing tubing length and keeping the syringes adjacent and horizontal to the microfluidic chip further minimizes gravity-driven flow disturbances. No evidence of on-chip flow instability is observed at any flow rate by visualization and tracing of PEC droplets flow.

5.3.2 Pipette mixing

Pipette mixing was used to study the influence of moderate Reynolds-number mixing flows on PEC formation and aging. Mixtures were prepared by diluting the proper volumes of NaCl stock into Milli-Q water in a 1.5 mL MaxyClear™ microcentrifuge tube (Axygen Scientific). Next, the proper volume of PAA stock was added and mixed thoroughly by aspirating at least 5 times. Finally, the proper volume of PAH stock was added and aspirated exactly 5 times to achieve a total mixture volume of 1 mL. As quickly as possible, the sample tube was gently capped and inverted once. Aging time $t_{\text{pipette}} = 0$ was recorded as the moment the inversion is finished.

5.3.3 Vortex mixing

Vortex mixing was used to study the effect of turbulent mixing flows on PEC formation and aging. Solutions were prepared using the same protocol as pipette mixing, with the tube placed immediately onto a Fisherbrand™ 120 V analog variable-speed vortex mixer at the highest speed setting (3200 rpm). Aging time $t_{\text{vortex}} = 0$ was recorded as the moment the microcentrifuge tube is removed from the vortex mixer.

5.4 Structural characterization

5.4.1 Optical microscopy

Manual brightfield imaging of samples during microfluidic mixing was conducted on an Olympus IX71 Inverted Microscope in bright-field mode with a 40× air objective and 1.6 optical zoom (NA, pixel size) at room temperature. For droplet imaging, videos were collected at 10 Hz so as not to capture droplets on multiple video frames. The flow rate was maintained at 0.5 $\mu\text{L}/\text{min}$, keeping the focal plane 19 μm above the bottom of the mixing channel (near the center line). For sediment imaging, videos were collected at 8.8 Hz at various fixed flow rates, and the focal plane was maintained at the bottom of the mixing channel. For static imaging of structure after pipette or vortex mixing, a mixture of solid and fluid sample is gently spooned out of the microcentrifuge tube onto a glass slide directly after mixing, and imaged within 30 seconds after mixing.

An automated optical microscope was used to track structural relaxation. Mixed solutions were immediately transferred using a 5 mL pipetter to a 96-Well Krystal™ Glass Bottom Imaging Plate (Thomas Scientific, Swedesboro, NJ), surrounded by wells containing 350 μL of water, and lidded during the duration of the experiment. The covered well-plate minimizes evaporation and eliminates flow and confinement issues during sample relaxation. Samples are imaged directly in the well-plate using a Zeiss Axio Observer 7 microscope outfitted with a computer-controlled motorized sample stage and motorized auto-focus objectives, and recorded with an Axiocam 702 monochromatic camera under brightfield illumination.

Video imaging was used to track aging of individual structures. For this purpose, only 100 μL of solution is transferred to the 96-well plate for each sample to improve light penetration. A 20× air objective (NA 0.6, 0.293 $\mu\text{m}/\text{pixel}$) is used for imaging, with auto-focus adjusted to 0.5 μm above the well bottom. Images are

taken with automatic exposure every 30 seconds until the structure has relaxed.

For tiled images of entire wells, 100 μL of solution is transferred to the 96-well plate for each sample. Well plate position is calibrated using the Zeiss ZEN software standard procedure. Since tiled images are used for multi-day tracking of relaxation, the well-plate lid is secured with parafilm (Bemis Company, Neenah, WI) and tape to minimize evaporation. A tiled region of each well consists of 77 image tiles with 20% overlap between them, using a 10× air objective (NA 0.3, 0.590 $\mu\text{m}/\text{pixel}$). A sequence of scans is executed automatically, with a single channel image of each well complete in roughly one minute. A composite image of each complete well at each time point is generated using the Processing Module in Zen to merge the fields of view.

5.4.2 Visual observation of morphology

Aggregates are visible to the naked eye when larger than several 10s of microns, or $\sim 30\text{-}50$ μm in size,⁷⁵ ($\sim 15\text{-}35$ individual droplet diameters, see Section 2.2.1). The eye can therefore differentiate between formation of a turbid coacervate emulsion and an aggregating emulsion above this length scale. Morphology is immediately observed in bright lighting at $t = 0$. Visual observation is necessary when time resolution mattered more than the ability to see structures smaller than 10s of μm , which is particularly important for bulk mixing (i.e. Figure 2). Visual observations reported in this work are confirmed by multiple repetitions per mixture, as well as blind spot-check tests in which another scientist differentiates aggregating samples while oblivious to their composition.

Author Contributions

CERE and MEH conceptualized the study, designed the experiments, interpreted the data, and wrote the manuscript. CERE, KLL, and YL performed the experiments. CERE analyzed the data. All authors have given approval to the final manuscript.

Conflicts of interest

The authors declare no competing financial interest.

Acknowledgements

This work was supported by the National Science Foundation Materials Research Science and Engineering Center at UC Santa Barbara (DMR-1720256, IRG-3). CERE also acknowledges support from the Department of Defense (DoD) through the National Defense Science and Technology (NDSEG) Fellowship program. YL acknowledges partial support from the Otis Williams Postdoctoral Fellowship from the Division of Mathematical, Life, and Physical Sciences in the College of Letters and Science. The authors acknowledge the use of the Microfluidics Laboratory and Innovation Workshop within the California NanoSystems Institute, supported by the University of California, Santa Barbara and the University of California, Office of the President.

References

- 1 Y. Shin and C. P. Brangwynne, *Science*, 2017, **357**, eaaf4382.

- 2 S. Alberti, A. Gladfelter and T. Mittag, *Cell*, 2019, **176**, 419–434.
- 3 M. Feric, N. Vaidya, T. S. Harmon, D. M. Mitrea, L. Zhu, T. M. Richardson, R. W. Kriwacki, R. V. Pappu and C. P. Brangwynne, *Cell*, 2016, **165**, 1686–1697.
- 4 J. Sheu-Gruttadauria and I. J. MacRae, *Cell*, 2018, **173**, 946–957.
- 5 H. Jiang, S. Wang, Y. Huang, X. He, H. Cui, X. Zhu and Y. Zheng, *Cell*, 2015, **163**, 108–122.
- 6 G. C. Yeo, F. W. Keeley and A. S. Weiss, *Advances in Colloid and Interface Science*, 2011, **167**, 94–103.
- 7 L. D. Muiznieks, J. T. Cirulis, A. van der Horst, D. P. Reinhardt, G. J. Wuite, R. Pomès and F. W. Keeley, *Matrix Biology*, 2014, **36**, 39–50.
- 8 J. B. Woodruff, B. F. Gomes, P. O. Widlund, J. Mahamid, A. Honigmann and A. A. Hyman, *Cell*, 2017, **169**, 1066–1077.
- 9 J. H. Waite, *Structure, cellular synthesis and assembly of biopolymers*, 1992, 27–54.
- 10 W. R. Wonderly, T. T. Nguyen, K. G. Malollari, D. DeMartini, P. Delparastan, E. Valois, P. B. Messersmith, M. E. Helgeson and J. H. Waite, *Matter*, 2022.
- 11 J. Newar and A. Ghatak, *Langmuir*, 2015, **31**, 12155–12160.
- 12 P. Mohammadi, A. S. Aranko, L. Lemetti, Z. Cenev, Q. Zhou, S. Virtanen, C. P. Landowski, M. Penttilä, W. J. Fischer, W. Wagermaier and M. B. Linder, *Communications Biology*, 2018, **1**, 1–12.
- 13 L. Lemetti, S.-P. Hirvonen, D. Fedorov, P. Batys, M. Sammalkorpi, H. Tenhu, M. B. Linder and A. S. Aranko, *European Polymer Journal*, 2019, **112**, 539–546.
- 14 J. Deng and A. Walther, *Chem*, 2020, **6**, 3329–3343.
- 15 P. Zhang, K. Shen, N. M. Alsaifi and Z.-G. Wang, *Macromolecules*, 2018, **51**, 5586–5593.
- 16 L. Li, S. Srivastava, M. Andreev, A. B. Marciel, J. J. de Pablo and M. V. Tirrell, *Macromolecules*, 2018, **51**, 2988–2995.
- 17 J. Lou, S. Friedowitz, J. Qin and Y. Xia, *ACS Central Science*, 2019, **5**, 549–557.
- 18 L. Li, S. Srivastava, S. Meng, J. M. Ting and M. V. Tirrell, *Macromolecules*, 2020, **53**, 7835–7844.
- 19 M. Nguyen, N. Sherck, K. Shen, C. E. Edwards, B. Yoo, S. Kohler, J. C. Speros, M. E. Helgeson, K. T. Delaney, M. S. Shell *et al.*, *Macromolecules*, 2022.
- 20 Y. Liu, B. Momani, H. H. Winter and S. L. Perry, *Soft Matter*, 2017, **13**, 7332–7340.
- 21 F. G. Hamad, Q. Chen and R. H. Colby, *Macromolecules*, 2018, **51**, 5547–5555.
- 22 S. Ali and V. M. Prabhu, *Gels*, 2018, **4**, 11.
- 23 J. Huang, F. J. Morin and J. E. Laaser, *Macromolecules*, 2019, **52**, 4957–4967.
- 24 P. C. Suarez-Martinez, P. Batys, M. Sammalkorpi and J. L. Lutkenhaus, *Macromolecules*, 2019, **52**, 3066–3074.
- 25 F. J. Morin, M. L. Puppo and J. E. Laaser, *Soft Matter*, 2021, **17**, 1223–1231.
- 26 Y. Luo, M. Gu, C. E. Edwards, M. T. Valentine and M. E. Helgeson, *Soft Matter*, 2022, **18**, 3063–3075.
- 27 H. Li, Y. Liu, A. Shetty and R. G. Larson, *Journal of Rheology*, 2022, **66**, 1067–1077.
- 28 V. A. Kabanov and A. B. Zezin, *Pure and Applied Chemistry*, 1984, **56**, 343–354.
- 29 N. Karibyants, H. Dautzenberg and H. Coelfen, *Macromolecules*, 1997, **30**, 7803–7809.
- 30 E. Dickinson, R. Miller, C. Sanchez, S. Despond, C. Schmitt and J. Hardy, in *Food Colloids*, 2001, pp. 332–342.
- 31 M. F. Butler, *Biomacromolecules*, 2002, **3**, 1208–1216.
- 32 H. Dautzenberg and J. Kriz, *Langmuir*, 2003, **19**, 5204–5211.
- 33 A. Zintchenko, G. Rother and H. Dautzenberg, *Langmuir*, 2003, **19**, 2507–2513.
- 34 M. Mihai, E. S. Dragan, S. Schwarz and A. Janke, *The Journal of Physical Chemistry B*, 2007, **111**, 8668–8675.
- 35 W. C. B. McTigue, E. Voke, L.-W. Chang and S. L. Perry, *Physical Chemistry Chemical Physics*, 2020, **22**, 20643–20657.
- 36 Y. Yuan, J. Gao, Y. Zhai, D. Li, C. Fu and Y. Huang, *Carbohydrate Polymers*, 2022, **287**, 119331.
- 37 X. Liu, M. Haddou, I. Grillo, Z. Mana, J.-P. Chapel and C. Schatz, *Soft Matter*, 2016, **12**, 9030–9038.
- 38 X. Liu, J.-P. Chapel and C. Schatz, *Advances in Colloid and Interface Science*, 2017, **239**, 178–186.
- 39 R. Takahashi, T. Narayanan and T. Sato, *The Journal of Physical Chemistry Letters*, 2017, **8**, 737–741.
- 40 H. Le Ferrand, M. Duchamp, B. Gabryelczyk, H. Cai and A. Miserez, *Journal of the American Chemical Society*, 2019, **141**, 7202–7210.
- 41 F. Weinbreck, R. Tromp and C. De Kruif, *Biomacromolecules*, 2004, **5**, 1437–1445.
- 42 C. Sanchez, G. Mekhloufi and D. Renard, *Journal of Colloid and Interface Science*, 2006, **299**, 867–873.
- 43 Z. Yan, J. Xue, M. Zhou, J. Wang, Y. Zhang, Y. Wang, J. Qiao, Y. He, P. Li, S. Zhang *et al.*, *Analytical Chemistry*, 2021, **93**, 2988–2995.
- 44 D. Salvatore, T. Croguennec, S. Bouhallab, V. Forge and T. Nicolai, *Biomacromolecules*, 2011, **12**, 1920–1926.
- 45 S. Lindhoud and M. A. C. Stuart, *Polyelectrolyte Complexes in the Dispersed and Solid State I*, 2012, 139–172.
- 46 N. Jemili, M. Fauquignon, E. Grau, N. Fatin-Rouge, F. Dole, J.-P. Chapel, W. Essafi and C. Schatz, *Polymers*, 2022, **14**, 2404.
- 47 R. Y. Lochhead and L. R. Huisinga, *Cosmetics and Toiletries*, 2005, **120**, 69–78.
- 48 S. Lankalapalli and V. Kolapalli, *Indian Journal of Pharmaceutical Sciences*, 2009, **71**, 481.
- 49 C. Schmitt and S. L. Turgeon, *Advances in colloid and interface science*, 2011, **167**, 63–70.
- 50 B. Valley, B. Jing, M. Ferreira and Y. Zhu, *ACS applied materials & interfaces*, 2019, **11**, 7472–7478.
- 51 R. F. Shamoun, H. H. Hariri, R. A. Ghostine and J. B. Schlenoff, *Macromolecules*, 2012, **45**, 9759–9767.
- 52 Q. Wang and J. B. Schlenoff, *Macromolecules*, 2014, **47**, 3108–3116.
- 53 E. Yildirim, Y. Zhang, J. L. Lutkenhaus and M. Sammalkorpi,

- ACS Macro Letters*, 2015, **4**, 1017–1021.
- 54 Y. Zhang, P. Batys, J. T. O’Neal, F. Li, M. Sammalkorpi and J. L. Lutkenhaus, *ACS central science*, 2018, **4**, 638–644.
- 55 L. Jawerth, E. Fischer-Friedrich, S. Saha, J. Wang, T. Franzmann, X. Zhang, J. Sachweh, M. Ruer, M. Ijavi, S. Saha *et al.*, *Science*, 2020, **370**, 1317–1323.
- 56 S. P. Danielsen, S. Panyukov and M. Rubinstein, *Macromolecules*, 2020, **53**, 9420–9442.
- 57 R. Chollakup, W. Smitthipong, C. D. Eisenbach and M. Tirrell, *Macromolecules*, 2010, **43**, 2518–2528.
- 58 D. Priftis and M. Tirrell, *Soft Matter*, 2012, **8**, 9396–9405.
- 59 R. Chollakup, J. B. Beck, K. Dirnberger, M. Tirrell and C. D. Eisenbach, *Macromolecules*, 2013, **46**, 2376–2390.
- 60 S. L. Perry, L. Leon, K. Q. Hoffmann, M. J. Kade, D. Priftis, K. A. Black, D. Wong, R. A. Klein, C. F. Pierce, K. O. Margosian *et al.*, *Nature Communications*, 2015, **6**, 1–8.
- 61 C. S. Cummings and A. C. Obermeyer, *Biochemistry*, 2018, **57**, 314–323.
- 62 S. Meng, J. M. Ting, H. Wu and M. V. Tirrell, *Macromolecules*, 2020, **53**, 7944–7953.
- 63 N. J. Sinha, K. C. Cunha, R. Murphy, C. J. Hawker, J.-E. Shea and M. E. Helgeson, *Biomacromolecules*, 2023, **24**, 3580–3588.
- 64 H. T. Oyama and C. W. Frank, *Journal of Polymer Science Part B: Polymer Physics*, 1986, **24**, 1813–1821.
- 65 C. Sanchez, G. Mekhloufi, C. Schmitt, D. Renard, P. Robert, C.-M. Lehr, A. Lamprecht and J. Hardy, *Langmuir*, 2002, **18**, 10323–10333.
- 66 A. I. Petrov, A. A. Antipov and G. B. Sukhorukov, *Macromolecules*, 2003, **36**, 10079–10086.
- 67 D. Burgess, *Journal of colloid and interface science*, 1990, **140**, 227–238.
- 68 M. Smoluchowski, *Z. Phys. Chem.*, 1917, **92**, 129–168.
- 69 T. R. Camp and S. P. C., *J. Boston Soc. Civ. Eng.*, 1943, **30**, 219–230.
- 70 M. Kato, T. W. Han, S. Xie, K. Shi, X. Du, L. C. Wu, H. Mirzaei, E. J. Goldsmith, J. Longgood, J. Pei *et al.*, *Cell*, 2012, **149**, 753–767.
- 71 A. Patel, H. O. Lee, L. Jawerth, S. Maharana, M. Jahnel, M. Y. Hein, S. Stoynov, J. Mahamid, S. Saha, T. M. Franzmann *et al.*, *Cell*, 2015, **162**, 1066–1077.
- 72 Y. Lin, Y. Fichou, Z. Zeng, N. Y. Hu and S. Han, *ACS Chemical Neuroscience*, 2020, **11**, 615–627.
- 73 A. R. Tejedor, R. Collepardo-Guevara, J. Ramirez and J. R. Espinosa, *The Journal of Physical Chemistry B*, 2023.
- 74 M. Linsenmeier, M. Hondele, F. Grigolato, E. Secchi, K. Weis and P. Arosio, *Nature Communications*, 2022, **13**, 3030.
- 75 F. Campbell and D. Green, *The Journal of physiology*, 1965, **181**, 576.
- 76 D. L. Perry, *Handbook of inorganic compounds*, CRC press, 2016.
- 77 P. Taylor, *Advances in colloid and interface science*, 1998, **75**, 107–163.
- 78 A. Veis and C. Aranyi, *The Journal of Physical Chemistry*, 1960, **64**, 1203–1210.
- 79 V. M. Syed and S. Srivastava, *ACS Macro Letters*, 2020, **9**, 1067–1073.
- 80 J. Goodwin and J. Mercer-Chalmers, *Modern Aspects of Colloidal Dispersions: Results from the DTI Colloid Technology Programme*, 1998, 61–75.
- 81 A. Deblais, M. A. Herrada, J. Eggers and D. Bonn, *Journal of Fluid Mechanics*, 2020, **904**, R2.
- 82 P. J. Dekker, M. A. Hack, W. Tewes, C. Datt, A. Bouillant and J. H. Snoeijer, *Physical review letters*, 2022, **128**, 028004.
- 83 M. A. Fardin, M. Hautefeuille and V. Sharma, *Soft Matter*, 2022, **18**, 3291–3303.
- 84 S. C. Varma, A. S. Rajput and A. Kumar, *Macromolecules*, 2022.